

Article

# Friction and Wear Properties of a Nanoscale Ionic Liquid-like GO@SiO<sub>2</sub> Hybrid as a Water-Based Lubricant Additive

Liang Hao<sup>1,†</sup>, Wendi Hao<sup>1</sup>, Peipei Li<sup>2,†</sup>, Guangming Liu<sup>3</sup>, Huaying Li<sup>3,\*</sup>, Abdulrahman Aljabri<sup>4</sup>   
and Zhongliang Xie<sup>5,\*</sup> 

<sup>1</sup> School of Mechano-Electronic Engineering, Xidian University, Xi'an 710071, China;

haoliang@xidian.edu.cn (L.H.); xdhaowendi@163.com (W.H.)

<sup>2</sup> School of Advanced Materials and Nanotechnology, Xidian University, Xi'an 710126, China; lip@xidian.edu.cn

<sup>3</sup> School of Materials Science and Engineering, Taiyuan University of Science and Technology, Taiyuan 030024, China; brightliu2008@126.com

<sup>4</sup> Department of Mechanical Engineering, Islamic University of Madinah, Medina 42351, Saudi Arabia; aaljabri@iu.edu.sa

<sup>5</sup> Department of Engineering Mechanics, Northwestern Polytechnical University, Xi'an 710072, China

\* Correspondence: huayne@163.com (H.L.); zlxie@nwpu.edu.cn (Z.X.)

† These authors contributed equally to this work.

**Abstract:** In this study, a nanoscale ionic liquid (NIL) GO@SiO<sub>2</sub> hybrid was synthesized by attaching silica nanoparticles onto graphene oxide (GO). It was then functionalized to exhibit liquid-like behavior in the absence of solvents. The physical and chemical properties of the synthesized samples were characterized by means of a transmission electron microscope, X-ray diffraction, Fourier transform infra-red, Raman spectroscopy, and thermogravimetric analysis. The tribological properties of the NIL GO@SiO<sub>2</sub> hybrid as a water-based (WB) lubricant additive were investigated on a ball-on-disk tribometer. The results illustrate that the NIL GO@SiO<sub>2</sub> hybrid demonstrates good dispersity as a WB lubricant, and can decrease both the coefficient of friction (COF) and wear loss.

**Keywords:** tribological tests; GO@SiO<sub>2</sub> hybrid; water-based lubricant; additive



**Citation:** Hao, L.; Hao, W.; Li, P.; Liu, G.; Li, H.; Aljabri, A.; Xie, Z. Friction and Wear Properties of a Nanoscale Ionic Liquid-like GO@SiO<sub>2</sub> Hybrid as a Water-Based Lubricant Additive. *Lubricants* **2022**, *10*, 125. <https://doi.org/10.3390/lubricants10060125>

Received: 29 April 2022

Accepted: 7 June 2022

Published: 13 June 2022

**Publisher's Note:** MDPI stays neutral with regard to jurisdictional claims in published maps and institutional affiliations.



**Copyright:** © 2022 by the authors. Licensee MDPI, Basel, Switzerland. This article is an open access article distributed under the terms and conditions of the Creative Commons Attribution (CC BY) license (<https://creativecommons.org/licenses/by/4.0/>).

## 1. Introduction

Lubricants have become essential in the modern manufacturing industry, reducing energy consumption and improving the surface finish of products and the reliability of the production process. Petroleum derivatives and functional additives, such as extreme pressure agents, antioxidants, detergents, dispersants, etc., constitute traditional lubricants which are environmentally unfriendly and detrimental to human health. With growing concerns of energy crises and environmental issues, “Green Manufacturing”, or “Environmentally Conscious Manufacturing”, has gained considerable attention [1,2]. Therefore, novel lubricants, which are environmentally friendly and effective, are imperative to be developed to substitute traditional oil-based lubricants.

Since water is of low cost with a high cooling capacity, water-based lubricants are potential candidates for novel lubricants. However, the weaknesses of water, such as low viscosity, its corrosive properties, and especially the low strength of water films, constitute major barriers for tribological applications [3,4]. In order to adjust and improve water-based lubricants, high-quality functional additives are of great significance. Among these functional additives, nano-materials are extensively investigated due to their distinctive physiochemical and mechanical properties [5–7]. In addition, nanoparticles can improve tribological properties by improving the viscosity of water and nanolubrication mechanisms [8,9]. Nanoparticles added, such as metals (e.g., Cu [10,11] and Cu–Al alloy [12]), metal oxides (e.g., CuO [13], Fe<sub>3</sub>O<sub>4</sub> [14], Al<sub>2</sub>O<sub>3</sub> [15,16], TiO<sub>2</sub> [17–19], and ZnO [20,21]), non-metal oxides (e.g., SiO<sub>2</sub> [22–24]), sulfides (e.g., MoS<sub>2</sub> [25,26] and WS<sub>2</sub> [27]) and rare

earth compounds (e.g.,  $\text{CeO}_2$  [28] and  $\text{BCeO}_3$  [29]), offer anti-wear properties and lower friction due to the formation of tribofilms, in addition to micro-bearing, polishing and mending [30]. However, the poor dispersity of these nanoparticles in base stocks fails to enhance their tribological properties. A typical technique to stabilize nanoparticles in base stocks is to use physical methods, chemical methods, and self-dispersed methods. Traditional physical suspension processes include mechanical stirring, ultrasonication ball mill, and high-pressure homogenization [31,32]. Chemical methods mean modifying the inorganic–organic interface by attaching different functional groups on the surface of the nanoparticles [33]. Current studies have also revealed that the dispersion of the stability of nanoparticles can also be enhanced via the structure regulation of nanoparticles [34].

He et al. [16] mechanically dispersed different sizes and concentrations of  $\text{Al}_2\text{O}_3$  nanoparticles in glycerol water-based lubricants using an ultrasonic probe. The synthesized suspensions were found to be stable for only 3 days. Wu et al. [35] prepared  $\text{TiO}_2$  nano-additive water-based lubricants by modifying  $\text{TiO}_2$  nanoparticles with polyethyleneimine (PEI), and the suspensions were only stable for 7 days. Gup et al. [36] used oleic acid and ionic liquid to engineer  $\text{ZnO}$  and  $\text{WS}_2$  nanoparticles as oil additives, and the nanolubricants stratified after 10 days. In addition, silane coupling agents, commonly employed to modify nanoparticles, failed to form enough steric repulsion to stabilize the nanolubricants for a long period due to their light molecular weights [14,37,38]. Man et al. synthesized novel  $\text{CuO}@$ Graphene and added PAO-6 oil, reducing COF by more than 50% with 0.5 wt.% [39]. Surface-functionalized nanoparticles with liquid-like behavior in the absence of solvent have been coined nanoscale ionic liquids, which are organic–inorganic hybrids comprising a nanoparticle core functionalized with a covalently tethered ionic corona and oppositely charged canopy. The physical properties (rheological and solubility) of the nanoscale ionic liquids can be engineered over a broad range by adjusting the chemical characteristics of the corona and canopy [40–42]. Li et al. [43] synthesized a nanoscale liquid-like  $\text{graphene}@$  $\text{Fe}_3\text{O}_4$  hybrid according to the nanoscale ionic liquid method, and identified excellent amphiphilicity. On the other hand, graphene-based nanolubricant additives have gained increasing attention because of their superior lubricating performance, as well as their green and dashless properties. Graphene-based nanocomposites reveal good lubrication properties due to their synergistic effects [44,45].

In this work, a new kind of graphene-based composite was synthesized and modified for a water-based nanolubricant additive with enhanced stability. Following Section 1, the rest of the paper is organized as follows. The detailed synthesis and functionalization process, tribological tests, and characterizations are given in Section 2. In Section 3, synthetic, modification and tribological results, as well as lubrication mechanisms, are presented. Finally, Section 4 provides conclusions.

## 2. Experimental Section

### 2.1. Materials

GO solutions (purity: >99%; content: 1.55%; thickness: 0.55–2 nm; size: 1–5  $\mu\text{m}$ ) were purchased from Best Material Co., Ltd. (Chengdu, China). Tetraethyl orthosilicate (TEOS, 99% purity), ammonia (25% aqueous solution) and ethanol (99% purity) were purchased from Tianjin Organics (Tianjin, China). 3-(Trihydroxysilyl)-1-propanesulfonic acid (30–35% in water) (SIT8378.3,  $(\text{CH}_3)_3\text{Si}(\text{CH}_2)_3\text{HSO}_3$ ) was obtained from Gelest Inc. (Shanghai, China), while Jeffamine M-2070 Polyetheramine ( $\text{CH}_3-(\text{OCH}_2\text{CH}_2)_6-(\text{OCH}_2\text{CH}-\text{CH}_3)_{35}-\text{NH}_2$ ) was from HengYu Trading Co., Ltd. (Guangzhou, China). A ferritic stainless steel (FSS 444) was used as a disk material (Taiyuan, China). All the disks were cut to 28 mm in diameter, 2 mm in thickness, and surfaces were ground to a roughness of 0.6  $\mu\text{m}$ . GCr15 steel balls with a diameter of 6 mm and an identical  $R_a$  of 0.02 mm were employed for the ball-on-disk tests. The Vickers hardness of the ball and disk were 790 HV and 168 HV0.1. The main chemical compositions of FSS 444 (wt.%) were as follows: C 0.0094, Si 0.084, Mn 0.064, Cr 18.4, Mo 1.81, Nb 0.22, and Fe balance.

## 2.2. Synthesis of the GO@SiO<sub>2</sub> Compound

Firstly, 400 mL ethanol, 25 mL GO solution, 21 mL ammonia were sequentially poured into a three-necked, round-bottomed flask and stirred at 700 rpm in a 50 °C water bath for 30 min. Secondly, 16.1 mL TEOS was added, and the chemical reaction (700 rpm stirring and 50 °C water bath) occurred for 2 h. Then, the black precipitate was collected by centrifugation and washed with ethanol three times. Finally, the wet precipitate was free-dried for 24 h to obtain the GO@SiO<sub>2</sub> compound.

## 2.3. Preparation of the Nanoscale Liquid-like GO@SiO<sub>2</sub> Hybrid

To begin with, 500 mg GO@SiO<sub>2</sub> was dispersed in 10 mL deionized water under sonication to obtain the GO@SiO<sub>2</sub> suspension, followed by dropwise adding 5 mL SIT8378.3 solution and stirring for 30 min. Then, the NaOH solution (1 mol L<sup>-1</sup>) was added until the pH became 7, and the solution was stirred at room temperature for 24 h. In order to remove the residual SIT 8378.3, the solution was dialyzed using a dialysis tube for 48 h and the deionized water was exchanged every 8 h. Next, a cation exchange resin was employed to remove the Na<sup>+</sup> ions to protonate the sulfonate group. Finally, the polymer chains were attached onto the functionalized GO@SiO<sub>2</sub> compound by dropwise injecting 10 wt.% Jeffamine M-2070 solution to neutralize all sulfonate groups connected to the surface of the GO@SiO<sub>2</sub> compound. Finally, the solution was dried to a constant weight under vacuum at 50 °C, and the nanoscale liquid-like GO@SiO<sub>2</sub> hybrid was obtained. A synthetic framework is illustrated in Figure 1.

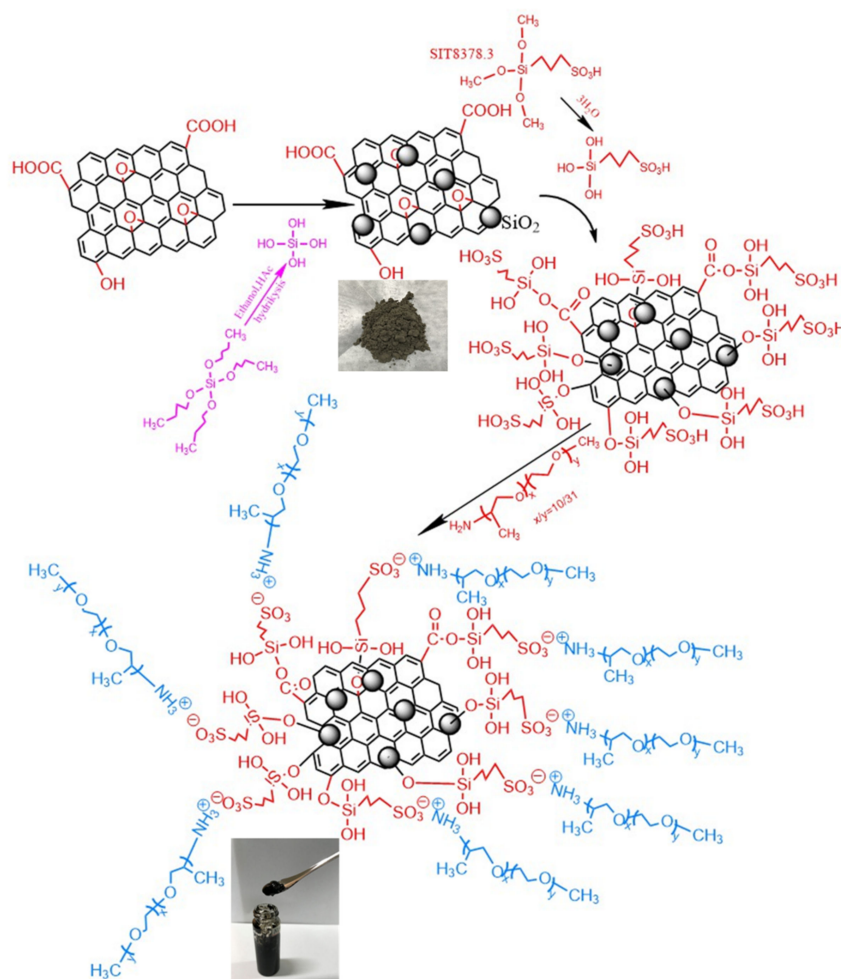


**Figure 1.** Synthetic framework of the nanoscale liquid-like GO@SiO<sub>2</sub> hybrid.

#### 2.4. Tribological Tests

The first step was to prepare the water-based (WB) lubricant (base fluid) and WB nanolubricants with different concentrations of the NIL GO@SiO<sub>2</sub> hybrid (1.0 wt.%, 2.0 wt.%, 4.0 wt.% and 8.0 wt.%). The detailed preparation process of all suspensions was as follows: (a) the WB lubricant consisted of 10.0 wt.% glycerol and 90.0 wt.% deionized water; (b) the base fluid was kept at 60 °C with an electromagnetic stirring heater, and proper amounts of NIL GO@SiO<sub>2</sub> were added into the base fluids under stirring for 30 min; (c) the suspensions were ultrasonicated for 30 min to obtain homogeneous WB nanolubricants.

Ball-on-disk tests were conducted on an Rtec MFT (multi-functional tribometer) 5000. Moving 10 mm away from the center of the disk, a normal force of 15 N was applied to the ball (equal to 1.6 GPa of the maximum Hertz contact stress) against the rotating disk at 200 rpm. The normal force employed to the ball holder was measured by an F<sub>z</sub> load cell installed above a spring. The friction force was generated by the combination of the rotating motion and the normal load. The coefficient of friction (COF) was calculated by the ratio between an F<sub>x</sub> load cell attached onto the ball holder and F<sub>z</sub>. The tribological trials were performed under different lubrication conditions for 20 min., and each test was repeated at least three times. During the tests, the COF variations were recorded automatically every two seconds. In addition, the wear of the balls after tests was evaluated by measuring the worn surface areas.

#### 2.5. Characterizations

The samples were prepared by placing a few drops of the GO and GO@SiO<sub>2</sub> dispersions onto a copper grid and then evaporating the solvent. Afterwards, transmission electron microscope (TEM) images were examined using JEM-2100F. The X-ray diffraction (XRD) analysis was conducted on a D8 Advance using Cu K $\alpha$  radiation. The measured  $2\theta$  values ranged from 10° to 80° and the scan step was 0.02. The chemical composition and physical properties of the GO, GO@SiO<sub>2</sub> compound and NIL GO@SiO<sub>2</sub> hybrid were investigated using a Fourier transform infra-red (FTIR, Nicolet iS50) spectra in the range of 4000 to 500 cm<sup>-1</sup>, and Raman spectroscopy (inVia). A Zeta potential analyzer (Zen3690) was used to characterize the dispersion stability. Thermogravimetric analysis (TGA) measurements were taken under Argon flow at a heating rate of 10 °C min<sup>-1</sup> using a STA 449F5 instrument.

The wear scars on the balls and the worn tracks of the disks were characterized using a Leica optical microscope (OM) and JSM-7800F field emission scanning electron microscope (FE-SEM) and EDS. In addition, atomic force microscopy (AFM) was carried out to measure the surface morphology of the wear tracks.

### 3. Results and Discussion

#### 3.1. Structural Analysis

The microstructures of the GO and GO@SiO<sub>2</sub> compounds were characterized by TEM, as shown in Figure 2. Figure 2a reveals that the GO nanosheets were efficiently exfoliated to form separate and transparent sheets. In addition, the dark color in the picture indicates that the GO nanosheets were folded. Compared with the GO (Figure 2a), the GO@SiO<sub>2</sub> compound was decorated with SiO<sub>2</sub> nanoparticles with a diameter of approximately 100 nm, in which the SiO<sub>2</sub> nanoparticles were sparsely attached onto the lamellae of GO, displaying no apparent nano-SiO<sub>2</sub> agglomeration.

The crystalline structures of GO, the GO@SiO<sub>2</sub> compound and the NIL GO@SiO<sub>2</sub> hybrid were analyzed by XRD. As shown in Figure 3, the diffraction of the GO peaks occurred at  $2\theta = 11.4^\circ$ , corresponding to the (0 0 2) plane. In addition, the characteristic diffraction peak at  $2\theta = 22^\circ$  can be assigned to the (1 1 1) plane reflection of SiO<sub>2</sub> according to PAN-ICSD NO.01-089-3435, which suggests that SiO<sub>2</sub> nanoparticles were successfully attached to the GO. Moreover, the XRD pattern of the NIL GO@SiO<sub>2</sub> hybrid revealed that GO@SiO<sub>2</sub> compounds retain their structural and size integrity after surface functionalization.

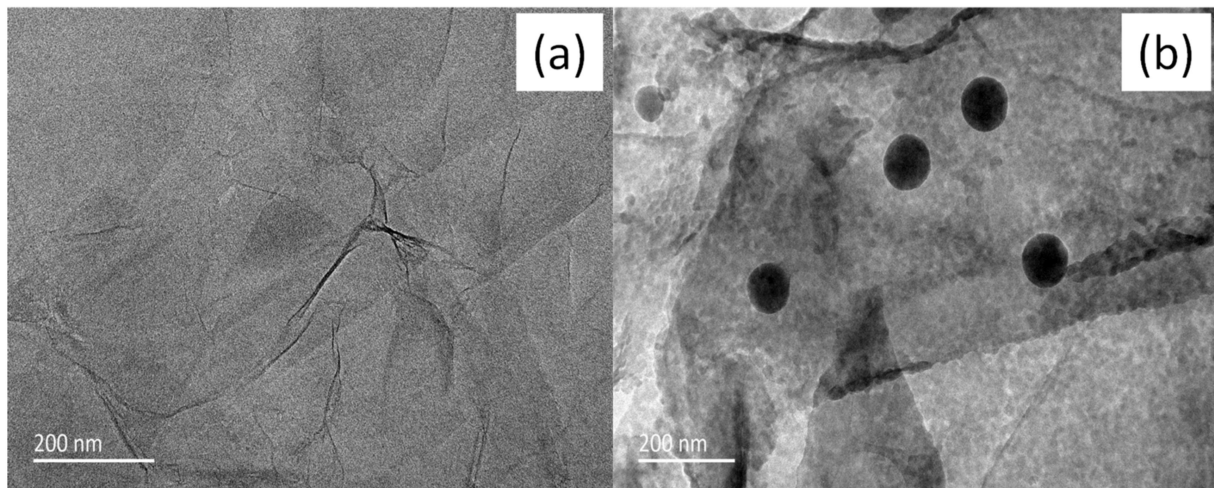


**Figure 2.** TEM images of the GO (a) and the GO@SiO<sub>2</sub> compound (b).

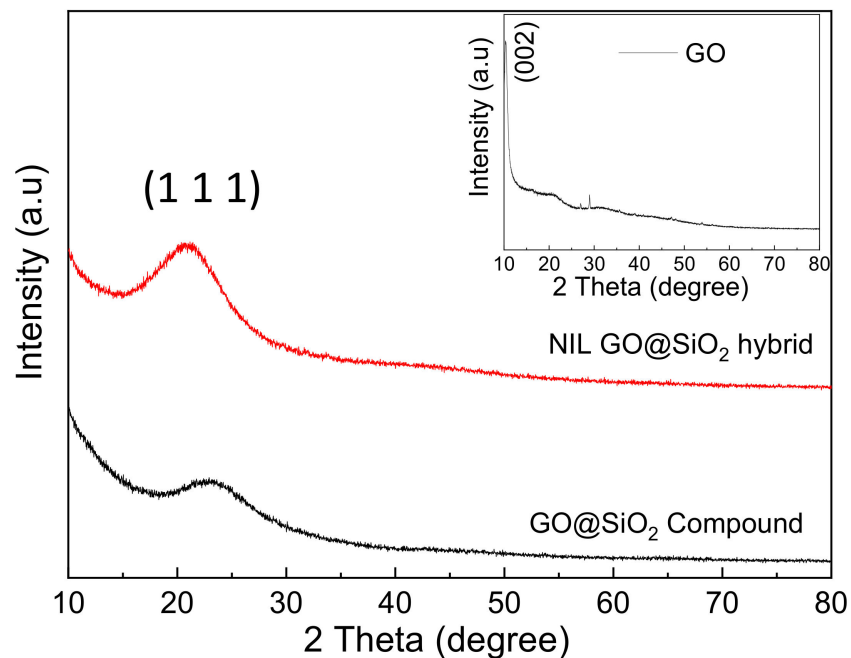


**Figure 3.** XRD patterns of GO and the GO@SiO<sub>2</sub> compound.

The FTIR spectra of GO, the GO@SiO<sub>2</sub> compound, and the NIL GO@SiO<sub>2</sub> hybrid are presented in Figure 4. The FTIR spectrum of GO reveals the presence of hydroxyl ( $\sim 3400\text{ cm}^{-1}$ ), epoxy ( $\sim 1177\text{ cm}^{-1}$ ), carboxyl ( $\sim 1733\text{ cm}^{-1}$ ), the O-H deformation ( $\sim 1049\text{ cm}^{-1}$ ), and the oxygenous groups ( $\sim 1624\text{ cm}^{-1}$ ) [46]. The intensities of these IR peaks dropped considerably after the attachment of the silica nanoparticles. In addition, the characteristic absorption peaks of Si-O ( $\sim 1105\text{ cm}^{-1}$ ) and Si-O-Si ( $\sim 1100\text{ cm}^{-1}$ ) were both observed, which confirms that silica was successfully deposited on the surface of the GO. As for the NIL GO@SiO<sub>2</sub> hybrid, the bands at  $\sim 2920\text{ cm}^{-1}$  and  $674\text{ cm}^{-1}$  were due to the C-H vibrations from the Jeffamine M-2070 and  $\text{SO}_3^{2-}$  from SIT 8378.3, respectively. Owing to the relatively small number of terminal ammonium groups present in the high molecular weight of the the Jeffamine M-2070, it is difficult to detect them in the FTIR spectra [47].

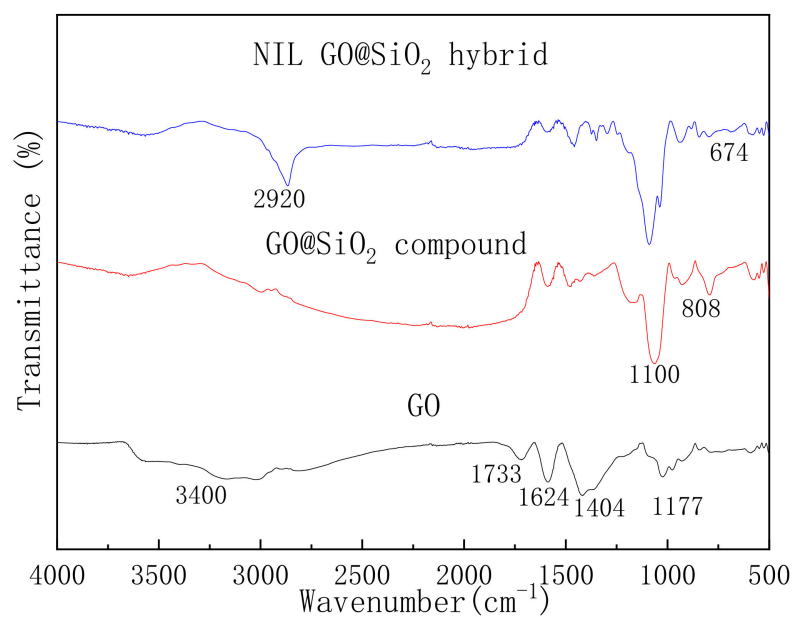


**Figure 4.** FTIR spectra of GO, GO@SiO<sub>2</sub> compound and NIL GO@SiO<sub>2</sub> hybrid.

To further investigate the layered and defect structure of carbonaceous materials, Raman spectroscopy was employed to explore the GO, the GO@SiO<sub>2</sub> compound and the NIL GO@SiO<sub>2</sub> hybrid. As shown in Figure 5, two bands around 1350 cm<sup>-1</sup> (D) and 1595 cm<sup>-1</sup> (G) represent the disorder of symmetry and crystallization, respectively [48], and are attributed to the activation of the first-order scattering process of sp<sup>3</sup> carbon and sp<sup>2</sup>-bonded carbon atoms in graphene sheets, respectively. The ratio of the D-band and G-band I(D)/I(G) is correlated to the ratio of disordered sp<sup>3</sup> and ordered sp<sup>2</sup> carbon domains. The higher the ratio of the D-band to G-band, the more defects in the carbon materials. Compared with GO (I<sub>D</sub>/I<sub>G</sub> = 0.96) and the GO@SiO<sub>2</sub> compound (I<sub>D</sub>/I<sub>G</sub> = 0.94), the NIL GO@SiO<sub>2</sub> hybrid increased to 1.02, implying that the sp<sup>2</sup> carbon domain decreased and new defects and polar groups were produced. In addition, the molecular charge transferred between M-2070 and the graphene also led to the increase in the I(D)/I(G) ratio [43].

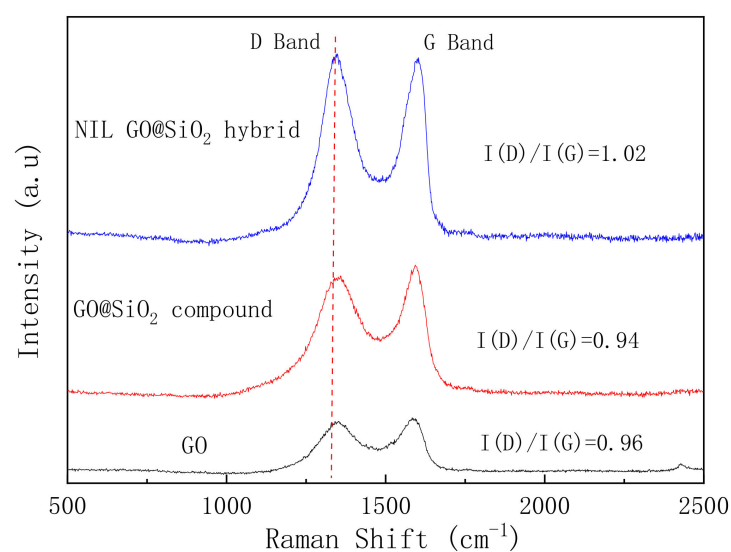


**Figure 5.** Raman spectra of GO, GO@SiO<sub>2</sub> compound and NIL GO@SiO<sub>2</sub> hybrid.

The content of the organic canopy attached to the NIL GO@SiO<sub>2</sub> hybrid affects the properties of the material. Therefore, TGA was conducted to evaluate the thermal stability and organic quantity of the material (Figure 6). Jeffamine M-2070 exhibited a relatively

higher decomposition at the temperature range of 300~420 °C, while the NIL GO@SiO<sub>2</sub> hybrid mainly underwent weight loss at the range of 280~360 °C. In addition, the GO@SiO<sub>2</sub> compound showed gradual weight loss up to approximately 14.5% until 600 °C, while the decomposition residual of the M-2070 was roughly 6.9%. Most especially, the TGA trace under Argon flow demonstrated that the NIL GO@SiO<sub>2</sub> hybrid is virtually solvent-free and a new hybrid, and is not a simple mixture of the M-2070 and GO@SiO<sub>2</sub> compound. As a result, it can be estimated that the organic component (surface functionalization groups) in the hybrid accounted for roughly 77.9%.

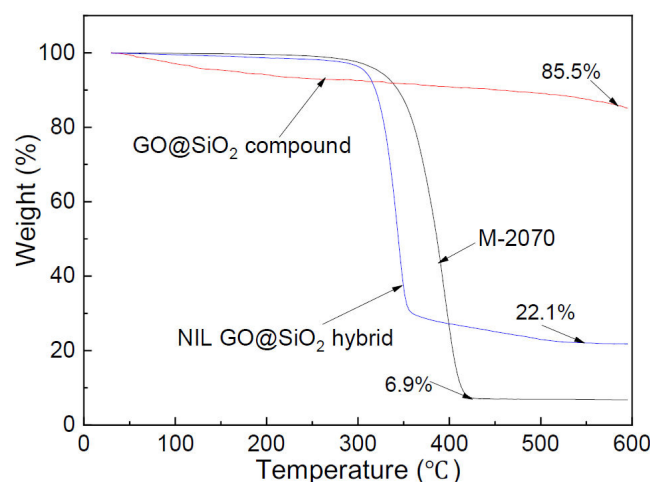


**Figure 6.** TGA curves of M-2070, GO@SiO<sub>2</sub> compound and NIL GO@SiO<sub>2</sub> hybrid.

### 3.2. Dispersion Stability

Since nanoparticles have a tendency to agglomerate, stability is a key issue for nanolubricants. The state of the nanoparticles results from a combined effect of the van der Waals attraction force and the electrical double-layer repulsive force [49]. The zeta potential (ZP) is an important and measurable indicator of the stability of colloids, and its magnitude reveals the degree of electrostatic repulsion between adjacent charged particles. High ZP implies highly charged particles, which prevents the aggregation of the particles due to electric repulsion, while low ZP implies that attraction overcomes repulsion, leading to coagulation. Figure 7 shows the ZP of nanolubricants with the GO@SiO<sub>2</sub> compound and the NIL GO@SiO<sub>2</sub> hybrid, respectively. The absolute ZP value (−45.8 mV) of the GO@SiO<sub>2</sub> hybrid dispersion was greater than that (−28.2 mV) of the GO@SiO<sub>2</sub> compound dispersion. Therefore, the surface functionalization of GO@SiO<sub>2</sub> by the NIL method improved the dispersion stability in the water-based lubricant.

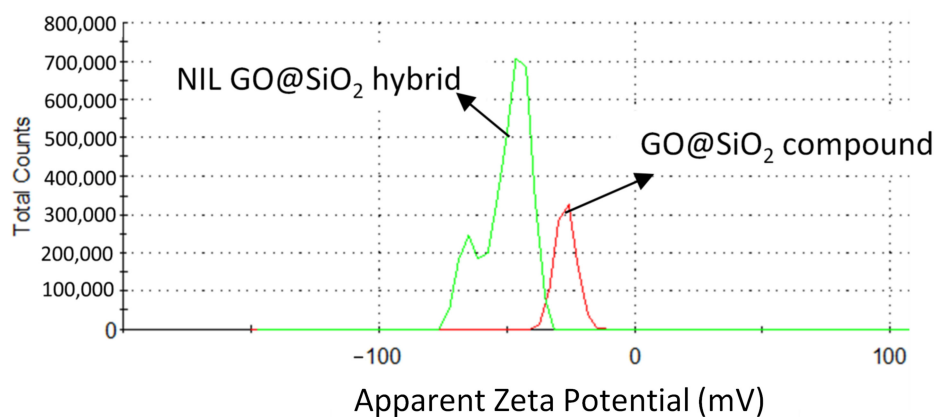


**Figure 7.** Zeta potential of nanolubricants with the GO@SiO<sub>2</sub> compound and the NIL GO@SiO<sub>2</sub> hybrid.

### 3.3. Tribological Properties

The friction and wear properties of the NIL GO@SiO<sub>2</sub> hybrid as the additive in the water-based lubricant were investigated by ball-on-disk tests. From Figure 8a, the in situ COF curves versus time revealed that the COF slightly varied from the start to the end in each scenario. It can be seen that the COF was relatively high under the lubrication of the water-based stock; however, 1.0 wt.% NIL GO@SiO<sub>2</sub> hybrid lubricant made the COF slightly fluctuate and hardly improved the lubrication performance. As the concentration of the water-based lubricant continuously increased, although the COF curve varied, it proceeded to be lower than that of the water-based stock. In particular, the COF values of 4.0 and 8.0 wt.% concentrations presented the comparatively lowest level of all scenarios. The AFC (average friction coefficient) and AWS (area of wear scar) of the balls are shown in Figure 8b. It can be seen that the addition of the NIL GO@SiO<sub>2</sub> hybrid was able to ameliorate the tribological performance by reducing the AFC and AWS. In contrast, the best lubrication performance was obtained at 4.0 wt.% hybrid concentration, in which the AFC and AWS were 0.33 and 0.084  $\mu\text{m}^2$ , respectively. Compared with the WB lubricant, these two values were reduced by 20.7% and 36.6%, respectively.

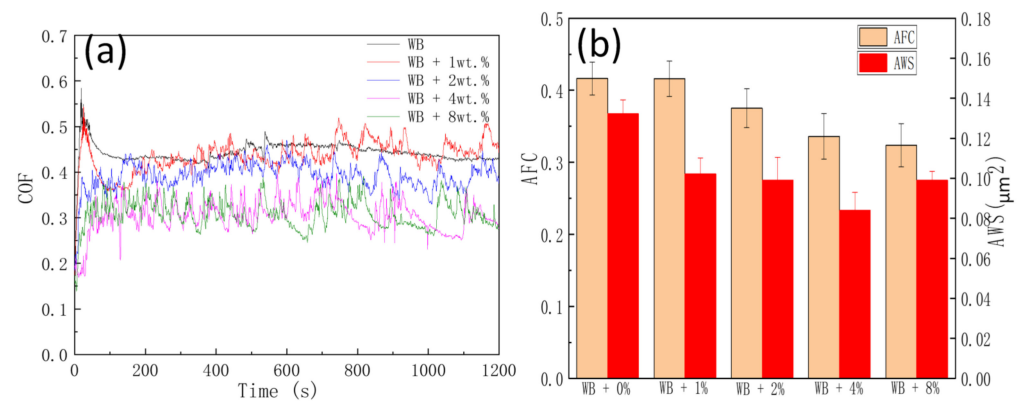


**Figure 8.** (a) COF versus time and (b) AFC and AWS lubricated by different concentrations.

As shown in Figure 9, wear tracks lubricated by the different concentrations of WB nanolubricants were characterized by AFM. It is evident that the addition of NIL GO@SiO<sub>2</sub> hybrid flattened the surface roughness. Deep grooves were generated under the lubrication of the WB lubricant with the surface roughness ( $R_a$ ) at about 700 nm (Figure 9a). Additionally, the addition of the NIL GO@SiO<sub>2</sub> hybrid decreased the track roughness at all concentrations tested (Figure 9b–e), which was about 100 nm. As a result, abrasive polishing was ascribed to be one of the lubrication forms of the NIL GO@SiO<sub>2</sub> hybrid [50].

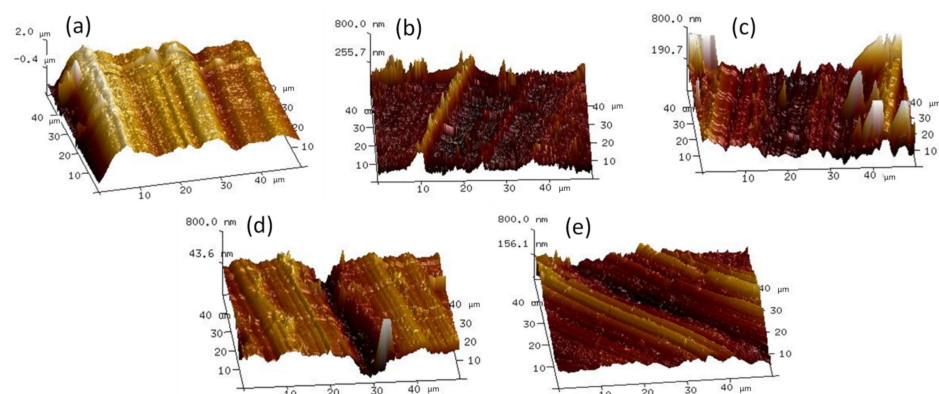


**Figure 9.** AFM images of wear tracks lubricated by (a) the WB lubricant, (b) 1.0 wt.%, (c) 2.0 wt.%, (d) 4.0 wt.%, and (e) 8.0 wt.% NIL GO@SiO<sub>2</sub>.

### 3.4. Inquiry of Lubrication Mechanisms

The lubrication enhancement of nanoparticles can be primarily divided into four mechanisms, including the micro-bearing effect, the self-repairing effect, tribo-film, and the polishing effect [51]. As the ball was pressed against the rotating disk under the nanolubricants, the GO@SiO<sub>2</sub> nanoparticles were dragged into the engaging surfaces with the base fluid, leaving deposits on the mating surfaces.

In order to understand the mechanisms of friction reduction and anti-wear for the NIL GO@SiO<sub>2</sub> hybrid, FE-SEM morphologies of the worn track lubricated under the different concentrations are displayed in Figure 10. Spherical nanoparticles can be discerned at all concentrations; these are the silica nanoparticles attached to the GO. The friction reduction was less obvious at low concentrations (1.0 wt.% and 2.0 wt.%), because there were limited nanoparticles deposited on the mating surfaces (Figure 10a,b). When the concentration increased to 4.0 wt.% and 8.0 wt.%, both friction reduction and anti-wear were reduced more than 20%. Furthermore, the shape and size of the nanoparticles were well maintained after the wear tests, which implies that the NIL GO@SiO<sub>2</sub> hybrid may have a typical micro-bearing effect in common cases [52]. Moreover, graphene also promotes relative sliding between the mating surfaces.

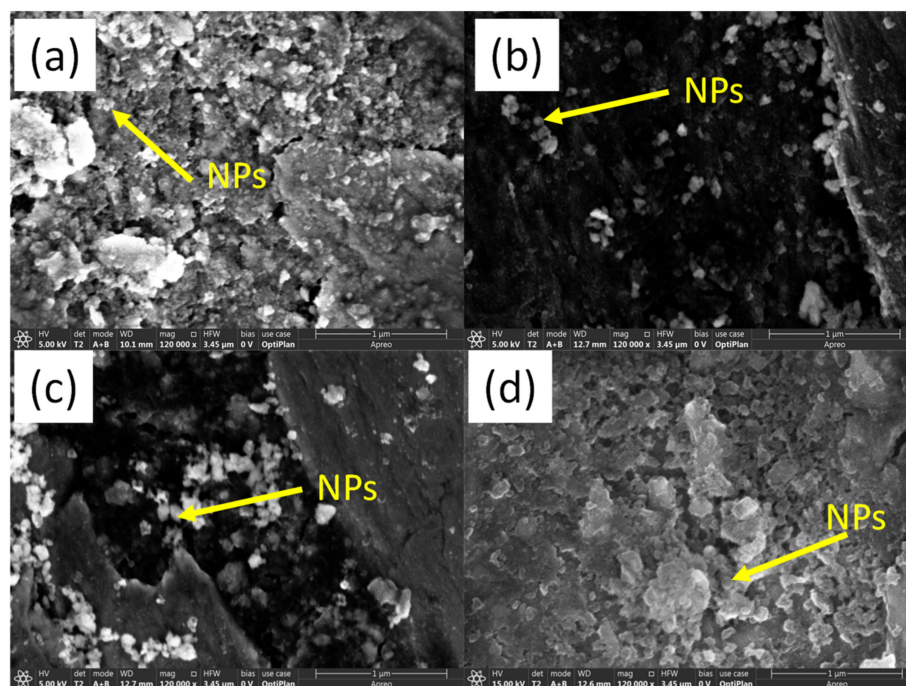


**Figure 10.** FE-SEM images of the worn surfaces on disks lubricated by (a) 1.0 wt.%, (b) 2.0 wt.%, (c) 4.0 wt.%, and (d) 8.0 wt.% NIL GO@SiO<sub>2</sub>.

FE-SEM image of the wear track lubricated by the 4.0% NIL GO@SiO<sub>2</sub> hybrid and a point element analysis are given in Figure 11. The spherical particles (bright color) can be discerned, and the EDS spectra analysis (Figure 11b) reveals Si (wt.% 2.76) and C (wt.% 2.49) elements on the worn track, which illustrates that the NIL GO@SiO<sub>2</sub> hybrid was embedded onto the steel substrate under high contact pressure. This indicates that the spherical SiO<sub>2</sub> nanoparticles in the lubricant can roll between the rubbing surfaces during the friction process. The graphene deposited onto the rubbing surfaces also plays a role in anti-wear and friction reduction. At the later stage, the hybrid could take effect and avoid the direct steel-to-steel contact to reduce wear. In future, more exquisite techniques (focused ion beam—FIB) should be applied to characterize the lubrication films formed due to nanoparticles. Furthermore, Bao and our former findings [24,53] demonstrate that there is no chemical reaction of SiO<sub>2</sub> nanoparticles in the tribofilms, and the lubrication effect is only a physical effect.

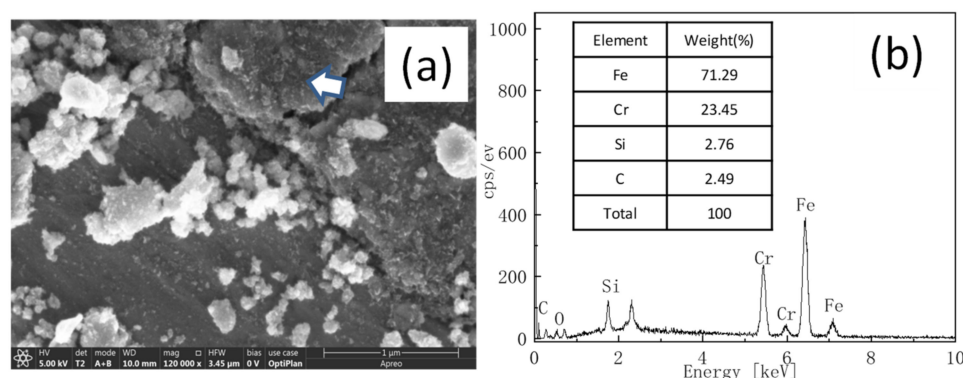


**Figure 11.** (a) FE-SEM image of the worn surfaces lubricated by 4.0 wt.% NIL GO@SiO<sub>2</sub> and (b) the point element analysis labeled in (a).

Therefore, the mechanisms responsible for the NIL GO@SiO<sub>2</sub> hybrid's ability to reduce friction and wear can be attributed to a synergy of mechanisms. Firstly, the nanoscale ionic liquid-functionalized GO@SiO<sub>2</sub> compound restrained the agglomeration of GO@SiO<sub>2</sub> in the water-based fluid; secondly, when the NIL GO@SiO<sub>2</sub> hybrid WB nanolubricants were used, some nanoparticles were embedded onto the disk surface, acting as micro-bearings. Additionally, the NIL GO@SiO<sub>2</sub> hybrid could be pressed to form tribofilms, preventing direct steel-to-steel contact. Thirdly, during the stable period, the nanoparticles refilled the friction pair surfaces (so-called "mending"), and the replenishment and loss of nanoparticle obtained a balance. The nanolubricants also took away debris and friction heat to avoid welding between asperities. Thus, the NIL GO@SiO<sub>2</sub> hybrid exhibits a good tribological performance.

#### 4. Conclusions

In this work, silica nanoparticles with a diameter of 100 nm were successfully attached onto graphene oxide. Then, based on the nanoscale ionic liquid method, the GO@SiO<sub>2</sub> compound was functionalized to obtain a liquid-like GO@SiO<sub>2</sub> hybrid. The lubrication performance of the NIL GO@SiO<sub>2</sub> hybrid as a water-based lubricant was investigated using a ball-on-disk tribometer. Based on the aforementioned analysis, the following conclusions were obtained:

1. The as-synthesized NIL GO@SiO<sub>2</sub> hybrid consisted of approximately 77.9% organic components and 22.1% inorganic components, exhibiting good dispersity and stability as a WB lubricant;
2. The addition of the NIL GO@SiO<sub>2</sub> hybrid reduced the COF and AWS at all tested concentrations. Compared with the WB lubricant, the 4.0 wt% hybrid nanolubricant lowered COF and AWS by 20.7% and 36.6%, respectively;
3. The tribological enhancement of the NIL GO@SiO<sub>2</sub> hybrid can be explained by the synergistic mechanisms of micro-rolling, polishing and mending in the GO@SiO<sub>2</sub> compound.

**Author Contributions:** Conceptualization, L.H. and P.L.; methodology, G.L.; software, W.H.; validation, H.L.; formal analysis, A.A.; investigation, Z.X.; resources, L.H.; data curation, W.H.; writing—original draft preparation, L.H.; writing—review and editing, P.L.; visualization, W.H.; supervision, G.L.; project administration, L.H.; funding acquisition, L.H., H.L. and Z.X. All authors have read and agreed to the published version of the manuscript.

**Funding:** This research was funded by National Natural Science Foundation of China (Grant No. 51904217), Natural Science Foundation of Shaanxi Province (Grant No. 2020JQ-294), Science and Technology Innovation Project of Educational Commission of Shanxi Province (Grant No. 2020L0333) and Natural Science Basic Research Program of Shaanxi (Program No. 2022JM-003).

**Institutional Review Board Statement:** Not applicable.

**Informed Consent Statement:** Not applicable.

**Data Availability Statement:** Not applicable.

**Conflicts of Interest:** The authors declare no conflict of interest.

### Nomenclature

NIL	nanoscale ionic liquid
English Symbols	
FSS	Ferritic Stainless Steel
GO	Graphene Oxide
TEO	Tetraethyl orthosilicate
WB	water-based
MFT	multi-functional tribometer
COF	coefficient of friction
TEM	Transmission Electron Microscope
XRD	X-ray diffraction
FTIR	Fourier Transform Infra-Red
TGA	Thermogravimetric analyzer
OM	Optical Microscope
AFM	Atomic Force Microscopy

### References

1. Wu, H.; Zhao, J.; Luo, L.; Huang, S.; Wang, L.; Zhang, S.; Jiao, S.; Huang, H.; Jiang, Z. Performance Evaluation and Lubrication Mechanism of Water-Based Nanolubricants Containing Nano-TiO<sub>2</sub> in Hot Steel Rolling. *Lubricants* **2018**, *6*, 57. [\[CrossRef\]](#)
2. Rahman, M.H.; Warneke, H.; Webbert, H.; Rodriguez, J.; Austin, E.; Tokunaga, K.; Rajak, D.K.; Menezes, P.L. Water-Based Lubricants: Development, Properties, and Performances. *Lubricants* **2021**, *9*, 73. [\[CrossRef\]](#)
3. Tomala, A.; Karpinska, A.; Werner, W.S.M.; Olver, A.; Störi, H. Tribological properties of additives for water-based lubricants. *Wear* **2010**, *269*, 804–810. [\[CrossRef\]](#)
4. Xie, Z.; Zhu, W. An investigation on the lubrication characteristics of floating ring bearing with consideration of multi-coupling factors. *Mech. Syst. Signal Process.* **2022**, *162*, 108086. [\[CrossRef\]](#)
5. Khalid Shafi, W.; Charoo, M.S. NanoLubrication Systems: An Overview. *Mater. Today Proc.* **2018**, *5*, 20621–20630. [\[CrossRef\]](#)
6. Jia, X.; Huang, J.; Li, Y.; Yang, J.; Song, H. Monodisperse Cu nanoparticles @ MoS<sub>2</sub> nanosheets as a lubricant additive for improved tribological properties. *Appl. Surf. Sci.* **2019**, *494*, 430–439. [\[CrossRef\]](#)
7. Darminesh, S.P.; Sidik, N.A.C.; Najafi, G.; Mamat, R.; Ken, T.L.; Asako, Y. Recent development on biodegradable nanolubricant: A review. *Int. Commun. Heat Mass Transf.* **2017**, *86*, 159–165. [\[CrossRef\]](#)
8. Wang, L.; Tieu, A.K.; Zhu, H.; Deng, G.; Cui, S.; Zhu, Q. A study of water-based lubricant with a mixture of polyphosphate and nano-TiO<sub>2</sub> as additives for hot rolling process. *Wear* **2021**, *477*, 203895. [\[CrossRef\]](#)
9. Thampi, A.D.; Prasanth, M.A.; Anandu, A.P.; Sneha, E.; Sasidharan, B.; Rani, S. The effect of nanoparticle additives on the tribological properties of various lubricating oils—Review. *Mater. Today Proc.* **2021**, *47*, 4919–4924. [\[CrossRef\]](#)
10. Guo, Z.; Zhang, Y.; Wang, J.; Gao, C.; Zhang, S.; Zhang, P.; Zhang, Z. Interactions of Cu nanoparticles with conventional lubricant additives on tribological performance and some physicochemical properties of an ester base oil. *Tribol. Int.* **2020**, *141*, 105941. [\[CrossRef\]](#)
11. Chen, X.; Han, Z.; Li, X.; Lu, K. Lowering coefficient of friction in Cu alloys with stable gradient nanostructures. *Sci. Adv.* **2016**, *2*, e1601942. [\[CrossRef\]](#) [\[PubMed\]](#)
12. Chen, X.; Han, Z.; Lu, K. Enhancing wear resistance of Cu–Al alloy by controlling subsurface dynamic recrystallization. *Scr. Mater.* **2015**, *101*, 76–79. [\[CrossRef\]](#)
13. Alves, S.M.; Mello, V.S.; Faria, E.A.; Camargo, A.P.P. Nanolubricants developed from tiny CuO nanoparticles. *Tribol. Int.* **2016**, *100*, 263–271. [\[CrossRef\]](#)
14. Atila Dinçer, C.; Yıldız, N.; Aydoğan, N.; Çalimli, A. A comparative study of Fe<sub>3</sub>O<sub>4</sub> nanoparticles modified with different silane compounds. *Appl. Surf. Sci.* **2014**, *318*, 297–304. [\[CrossRef\]](#)
15. Luo, T.; Wei, X.; Huang, X.; Huang, L.; Yang, F. Tribological properties of Al<sub>2</sub>O<sub>3</sub> nanoparticles as lubricating oil additives. *Ceram. Int.* **2014**, *40*, 7143–7149. [\[CrossRef\]](#)
16. He, A.; Huang, S.; Yun, J.H.; Wu, H.; Jiang, Z.; Stokes, J.; Jiao, S.; Wang, L.; Huang, H. Tribological Performance and Lubrication Mechanism of Alumina Nanoparticle Water-Based Suspensions in Ball-on-Three-Plate Testing. *Tribol. Lett.* **2017**, *65*, 40. [\[CrossRef\]](#)
17. Ingole, S.; Charanpahari, A.; Kakade, A.; Umare, S.S.; Bhatt, D.V.; Menghani, J. Tribological behavior of nano TiO<sub>2</sub> as an additive in base oil. *Wear* **2013**, *301*, 776–785. [\[CrossRef\]](#)
18. Wu, H.; Zhao, J.; Xia, W.; Cheng, X.; He, A.; Yun, J.H.; Wang, L.; Huang, H.; Jiao, S.; Huang, L.; et al. A study of the tribological behaviour of TiO<sub>2</sub> nano-additive water-based lubricants. *Tribol. Int.* **2017**, *109*, 398–408. [\[CrossRef\]](#)

19. Kong, L.; Sun, J.; Bao, Y.; Meng, Y. Effect of TiO<sub>2</sub> nanoparticles on wettability and tribological performance of aqueous suspension. *Wear* **2017**, *376*, 786–791. [[CrossRef](#)]
20. Gara, L.; Zou, Q. Friction and Wear Characteristics of Oil-Based ZnO Nanofluids. *Tribol. Trans.* **2013**, *56*, 236–244. [[CrossRef](#)]
21. Javed, R.; Usman, M.; Tabassum, S.; Zia, M. Effect of capping agents: Structural, optical and biological properties of ZnO nanoparticles. *Appl. Surf. Sci.* **2016**, *386*, 319–326. [[CrossRef](#)]
22. Peng, D.X.; Chen, C.H.; Kang, Y.; Chang, Y.P.; Chang, S.Y. Size effects of SiO<sub>2</sub> nanoparticles as oil additives on tribology of lubricant. *Ind. Lubr. Tribol.* **2010**, *62*, 111–120. [[CrossRef](#)]
23. Kumar, R.S.; Sharma, T. Stability and rheological properties of nanofluids stabilized by SiO<sub>2</sub> nanoparticles and SiO<sub>2</sub>-TiO<sub>2</sub> nanocomposites for oilfield applications. *Colloids Surf. A Physicochem. Eng. Asp.* **2018**, *539*, 171–183. [[CrossRef](#)]
24. Bao, Y.; Sun, J.; Kong, L. Effects of nano-SiO<sub>2</sub> as water-based lubricant additive on surface qualities of strips after hot rolling. *Tribol. Int.* **2017**, *114*, 257–263. [[CrossRef](#)]
25. Wu, H.; Johnson, B.; Wang, L.; Dong, G.; Yang, S.; Zhang, J. High-efficiency preparation of oil-dispersible MoS<sub>2</sub> nanosheets with superior anti-wear property in ultralow concentration. *J. Nanoparticle Res.* **2017**, *19*, 339. [[CrossRef](#)]
26. Forsberg, V.; Zhang, R.; Bäckström, J.; Dahlström, C.; Andres, B.; Norgren, M.; Andersson, M.; Hummelgård, M.; Olin, H. Exfoliated MoS<sub>2</sub> in Water without Additives. *PLoS ONE* **2016**, *11*, e0154522. [[CrossRef](#)]
27. Aldana, P.U.; Vacher, B.; Le Mogne, T.; Belin, M.; Thiebaut, B.; Dassenoy, F. Action Mechanism of WS<sub>2</sub> Nanoparticles with ZDDP Additive in Boundary Lubrication Regime. *Tribol. Lett.* **2014**, *56*, 249–258. [[CrossRef](#)]
28. Loya, A.; Stair, J.L.; Ren, G. Simulation and experimental study of rheological properties of CeO<sub>2</sub>-water nanofluid. *Int. Nano Lett.* **2015**, *5*, 1–7. [[CrossRef](#)]
29. Boshui, C.; Kecheng, G.; Jianhua, F.; Jiang, W.; Jiu, W.; Nan, Z. Tribological characteristics of monodispersed cerium borate nanospheres in biodegradable rapeseed oil lubricant. *Appl. Surf. Sci.* **2015**, *353*, 326–332. [[CrossRef](#)]
30. Shahnazar, S.; Bagheri, S.; Abd Hamid, S.B. Enhancing lubricant properties by nanoparticle additives. *Int. J. Hydrogen Energy* **2016**, *41*, 3153–3170. [[CrossRef](#)]
31. Chakraborty, S.; Panigrahi, P.K. Stability of nanofluid: A review. *Appl. Therm. Eng.* **2020**, *174*, 115259. [[CrossRef](#)]
32. Yu, F.; Chen, Y.; Liang, X.; Xu, J.; Lee, C.; Liang, Q.; Tao, P.; Deng, T. Dispersion stability of thermal nanofluids. *Prog. Nat. Sci. Mater. Int.* **2017**, *27*, 531–542. [[CrossRef](#)]
33. Wu, W.; Liu, J.; Li, Z.; Zhao, X.; Liu, G.; Liu, S.; Ma, S.; Li, W.; Liu, W. Surface-Functionalized NanoMOFs in Oil for Friction and Wear Reduction and Antioxidation. *Chem. Eng. J.* **2021**, *410*, 128306. [[CrossRef](#)]
34. Zhao, J.; Huang, Y.; He, Y.; Shi, Y. Nanolubricant additives: A review. *Friction* **2021**, *9*, 891–917. [[CrossRef](#)]
35. Wu, H.; Zhao, J.; Cheng, X.; Xia, W.; He, A.; Yun, J.H.; Huang, S.; Wang, L.; Huang, H.; Jiao, S.; et al. Friction and wear characteristics of TiO<sub>2</sub> nano-additive water-based lubricant on ferritic stainless steel. *Tribol. Int.* **2018**, *117*, 24–38. [[CrossRef](#)]
36. Guo, J.; Barber, G.C.; Schall, D.J.; Zou, Q.; Jacob, S.B. Tribological properties of ZnO and WS<sub>2</sub> nanofluids using different surfactants. *Wear* **2017**, *382*, 8–14. [[CrossRef](#)]
37. Sonn, J.S.; Lee, J.Y.; Jo, S.H.; Yoon, I.-H.; Jung, C.-H.; Lim, J.C. Effect of surface modification of silica nanoparticles by silane coupling agent on decontamination foam stability. *Ann. Nucl. Energy* **2018**, *114*, 11–18. [[CrossRef](#)]
38. Kang, T.; Jang, I.; Oh, S.-G. Surface modification of silica nanoparticles using phenyl trimethoxy silane and their dispersion stability in N-methyl-2-pyrrolidone. *Colloids Surf. A Physicochem. Eng. Asp.* **2016**, *501*, 24–31. [[CrossRef](#)]
39. Man, W.; Huang, Y.; Gou, H.; Li, Y.; Zhao, J.; Shi, Y. Synthesis of novel CuO@Graphene nanocomposites for lubrication application via a convenient and economical method. *Wear* **2022**, *498–499*, 204323. [[CrossRef](#)]
40. Rodriguez, R.; Herrera, R.; Archer, L.A.; Giannelis, E.P. Nanoscale Ionic Materials. *Adv. Mater.* **2008**, *20*, 4353–4358. [[CrossRef](#)]
41. Rodriguez, R.; Herrera, R.; Bourlinos, A.B.; Li, R.; Amassian, A.; Archer, L.A.; Giannelis, E.P. The synthesis and properties of nanoscale ionic materials. *Appl. Organomet. Chem.* **2010**, *24*, 581–589. [[CrossRef](#)]
42. Jespersen, M.L.; Mirau, P.A.; von Meerwall, E.; Vaia, R.A.; Rodriguez, R.; Giannelis, E.P. Canopy Dynamics in Nanoscale Ionic Materials. *ACS Nano* **2010**, *4*, 3735–3742. [[CrossRef](#)] [[PubMed](#)]
43. Li, P.; Zheng, Y.; Wu, Y.; Qu, P.; Yang, R.; Wang, N.; Li, M. A nanoscale liquid-like graphene@Fe<sub>3</sub>O<sub>4</sub> hybrid with excellent amphiphilicity and electronic conductivity. *New J. Chem.* **2014**, *38*, 5043–5051. [[CrossRef](#)]
44. Huang, J.; Li, Y.; Jia, X.; Song, H. Preparation and tribological properties of core-shell Fe<sub>3</sub>O<sub>4</sub>@C microspheres. *Tribol. Int.* **2019**, *129*, 427–435. [[CrossRef](#)]
45. Min, C.; He, Z.; Song, H.; Liang, H.; Liu, D.; Dong, C.; Jia, W. Fluorinated graphene oxide nanosheet: A highly efficient water-based lubricated additive. *Tribol. Int.* **2019**, *140*, 105867. [[CrossRef](#)]
46. He, D.; Peng, Z.; Gong, W.; Luo, Y.; Zhao, P.; Kong, L. Mechanism of a green graphene oxide reduction with reusable potassium carbonate. *RSC Adv.* **2015**, *5*, 11966–11972. [[CrossRef](#)]
47. Fernandes, N.; Dallas, P.; Rodriguez, R.; Bourlinos, A.B.; Georgakilas, V.; Giannelis, E.P. Fullerol ionic fluids. *Nanoscale* **2010**, *2*, 1653–1656. [[CrossRef](#)] [[PubMed](#)]
48. Zhang, J.; Li, P.; Zhang, Z.; Wang, X.; Tang, J.; Liu, H.; Shao, Q.; Ding, T.; Umar, A.; Guo, Z. Solvent-free graphene liquids: Promising candidates for lubricants without the base oil. *J. Colloid Interface Sci.* **2019**, *542*, 159–167. [[CrossRef](#)] [[PubMed](#)]
49. Kong, L.; Sun, J.; Bao, Y. Preparation, characterization and tribological mechanism of nanofluids. *RSC Adv.* **2017**, *7*, 12599–12609. [[CrossRef](#)]

50. Ali, M.K.A.; Xianjun, H.; Turkson, R.F.; Peng, Z.; Chen, X. Enhancing the thermophysical properties and tribological behaviour of engine oils using nano-lubricant additives. *RSC Adv.* **2016**, *6*, 77913–77924.
51. Azman, N.F.; Samion, S. Dispersion Stability and Lubrication Mechanism of Nanolubricants: A Review. *Int. J. Precis. Eng. Manuf. Green Technol.* **2019**, *6*, 393–414. [[CrossRef](#)]
52. Ranga Babu, J.A.; Kumar, K.K.; Srinivasa Rao, S. State-of-art review on hybrid nanofluids. *Renew. Sustain. Energy Rev.* **2017**, *77*, 551–565. [[CrossRef](#)]
53. Hao, L.; Wang, Z.; Zhang, G.; Zhao, Y.; Duan, Q.; Wang, Z.; Chen, Y.; Li, T. Tribological evaluation and lubrication mechanisms of nanoparticles enhanced lubricants in cold rolling. *Mech. Ind.* **2020**, *21*, 108–113. [[CrossRef](#)]